Gas-driven displacement of a liquid in a partially filled radial Hele-Shaw cell

Thomas Ward* and Andrew R. White

Department of Mechanical and Aerospace Engineering, North Carolina State University, Raleigh, North Carolina 27695-7910, USA

(Received 19 October 2010; revised manuscript received 4 March 2011; published 26 April 2011)

The displacement of liquids from confined geometries by using a gas phase is a problem that is relevant to many technologies. Efficient removal of the liquid phase is achieved when an extremely thin residual fluid film is produced as it is displaced. Here the dynamics of air, at constant pressure, displacing a glycerol-water drop in a radial Hele-Shaw cell is studied in this context at low Reynolds numbers. Empirically derived expressions relating the input parameters (fluid viscosity, pressure, and drop volume) to characteristic gas flow and liquid displacement rates, and the steady-state film thickness, are proposed and compared with experiments. The experiments consist of measuring cross-sectional areas of the penetrating gas (air) and displaced liquid using glycerol-water mixtures with viscosities ranging from 4 to 280 cSt and with inlet pressures ranging from 3.5 to 10.5 kPa at gap spacings of 50–100 μm. We estimate that the system produces residual film thicknesses in the range of 5–95 μm.

DOI: 10.1103/PhysRevE.83.046316 PACS number(s): 47.56.+r, 47.15.G−, 47.85.−g

I. INTRODUCTION

The displacement of a viscous fluid phase by a gas phase has been of interest to academics and industries for many years. There are several emerging and existing technologies where determining operating conditions that result in the efficient displacement of the more viscous phase is a desired outcome such as enhanced oil recovery processes that utilize CO_2 gas [1]. Other relevant technologies include the evaporation [2] or cooling [3] of a liquid phase by the penetrating gas phase so that it may be useful in a microgravity environment where, for example, processes involving buoyancy driven displacement, such as boiling, are difficult to engineer [4,5]. In each of these examples the fundamental question is how to efficiently displace liquids in small geometries by using a less viscous gas phase. In this paper a radial Hele-Shaw cell geometry with gap spacing b less than the capillary length $\ell_c = \sqrt{\gamma/\rho_L g}$ (where γ is the liquid-solid surface tension in air, ρ_L is the liquid phase density, and g is the gravitational acceleration constant) is used to experimentally study the dynamic penetration of a gas injected at a constant pressure into a finite volume of a viscous liquid, and to measure the residual thin film prior to bursting, that is, breakthough of the gas phase, at time t_{end}. The usual Saffman-Taylor fingering instability [6] occurs during the penetration of the gas into the liquid but the details of the fingering are not studied here. Instead we focus on the measurement of thin films and penetration rates of a less viscous fluid into a more viscous one in a radial Hele-Shaw cell geometry at low Reynolds numbers.

The desired experimental result is the displacement of a more viscous fluid by a less viscous fluid in a confined geometry where transport occurs in only the radial direction at the penetrating gas-liquid interface. But in practice this is never observed due to the formation of films of the more viscous fluid. Thick films can result in little radial displacement that can later develop into large droplets on the substrates where the maximum drop height is on the order of the capillary length [7]. In this paper it is assumed that the bursting time t_{end} is much shorter than the time required to produce a sufficient number of drops on the order of the gap spacing b (according to [7] this can take days for molecular scale films while in our experiments we typically observed droplet formation after bursting) and the film that results from the penetrating gas is assumed to be steady.

There is much literature on the subject of thin film formation by penetration of a viscous fluid phase with a less viscous one [8–13] and our discussion of these previous studies is to point out their similar conclusions. In general, all theories and experiments suggest that steady film thicknesses always scale like $h_\infty = C_0 \text{Ca}^{*n}$, where $\text{Ca}^* = U\mu_L/\gamma$ (here and throughout the paper asterisks denote a dimensionless variable) is the capillary number based on a steady velocity U and liquid viscosity μ_L. The steady film thickness is h_∞ and the power n and the coefficient C_0 are determined for a systems geometry and range of capillary numbers. For the film that forms when a bubble penetrates liquid in a tube the power is $n = 2/3$ for capillary numbers $\text{Ca}^* < 1 \times 10^{-3}$ [14]; the exponent power is slightly smaller at $n = 1/2$ for small capillary numbers $1 \times 10^{-3} < \text{Ca}^* < 1 \times 10^{-2}$ [15–17] and for $\text{Ca}^* \geqslant 1$ an asymptotic limit of h_∞ is approached [16]. A power of $n = 2/3$ was also determined for the problem of thin film formation due to displacement of a more viscous fluid by a less viscous fluid in a two-dimensional geometry [18–20].

It is more difficult to develop similar expressions relating the capillary number and film thickness for the problem of film formation due to fluid displacement in a *radial* Hele-Shaw geometry because the definition for a steady velocity is not easily accessible. Therefore, most previous Hele-Shaw studies in radial geometries focused on the Saffman-Taylor instability since a radial geometry allowed analysis of the moving front without interference from sidewalls [6,21–25].

In 1999 Carrillo *et al.* [26], through a combination of analysis and experimentation, studied fluid displacement driven by axial rotation in a radial Hele-Shaw geometry in the limit of low Reynolds and Rossby numbers. A study combining experiments and analysis of a similar system and for a wide range of rotation rates was performed in 2006 by Álvarez-Lacalle *et al.* [27]. In the inaugural studies of the axial rotation of a radial Hele-Shaw cell performed by Carillo *et al.* there were two conditions proposed: (1) a prewet

*tward@ncsu.edu

Hele-Shaw cell with a drop placed in the center and (2) a dry Hele-Shaw cell with all other conditions the same as the first. Their problem was unique because the authors were able to avoid the usual fingering instability by using rotation to generate centrifugal acceleration to displace the liquid phase, which subsequently syphoned the less viscous phase fluid (air) into the Hele-Shaw cell in their experiments. The ability to measure film thickness was possible in their system because the authors considered the displacement of a finite volume of liquid, denoted here as V_{liq}. The experimental analysis of a finite-liquid volume allows tracking of the outer and inner annular liquid radii, then with knowledge of the initial radius the authors determine a steady film thickness where they show that the residual film was less than 10% of the gap spacing. Note that in Carrillo *et al.* [26] an empirical capillary number was developed and we seek to do the same. We also form transport equations and develop expressions for displacements rates and film thickness based on the cross-sectional areas (penetrating gas and total) for the problem of a viscous fluid being displaced by a pressure driven less viscous one by developing empirical correlations based, in part, on the analysis of [26].

In the next section the problem description and cross-sectional area evolution equations are discussed. This is followed by an explanation of the experiments and details of the procedure. Then the experiments and results are analyzed qualitatively and quantitatively to describe data trends. In the last section we conclude with some remarks on the results and possible future experiments.

II. ANALYSIS

The purpose of this section is to develop an expression for the film thickness resulting from gas-driven displacement of a partially liquid-filled region in a radial Hele-Shaw cell by considering average displacements. To develop this equation we assume that the conserved volume of liquid forms a steady thin film as it is displaced liquid and gas phase liquid forms a steady thin film as it is displaced for the conserved volumes. Empirical correlations for the rate of displacement of the inner and outer cross-sectional areas are also introduced in the subsections that follow.

We begin with a discussion on the relative inner and outer annular radii a_1 and a_2, respectively, where the inner gas phase displaces the outer liquid phase fluid. We assume that the annular outer radius is simply a function of time $a_2(t)$ since the annular liquid is bounded by air. The inner gas creates a Saffman-Taylor instability as it penetrates the liquid phase, and for large amplitude instabilities, where a_1 is on the order of a_2, the approximation that a_2 is only a function of time will not hold. But it is observed to be accurate for the range of parameters presented in this study. We also only consider an average gas phase radius $\bar{a}_1(t)$ in the analysis by assuming that it is the sum of a uniform-average radius and a linear azimuthal disturbance $a_1(\theta,t) = \bar{a}_1(t) + \varepsilon(\theta,t)$ [22], where the disturbance is periodic in θ and possess azimuthal symmetry such that $\varepsilon(+\theta,t) = \varepsilon(-\theta,t)$ on some domain $\theta \in [-\pi,\pi]$.

Using this information we now consider an initially cylindrical-viscous Newtonian droplet of radius $a_2(0)$ concentrically confined between two parallel circular plates at a distance b apart where $b \ll \ell_c$ (see Fig. 1 for problem illustration) or equivalently the Bond number $\text{Bo}^* = (b/\ell_c)^2 \ll 1$. At time $t > 0$ a gas is injected into the center of the parallel plates at a constant pressure P_{gas} where the gage pressure is written as $\Delta P = P_{\text{gas}} - P_{\text{atm}}$ with P_{atm} equal to ambient atmospheric pressure. The injection pressure is assumed low, that is, $\Delta P/P_{\text{atm}} \ll 1$ so that the gas density and temperature are both considered constant throughout the displacement process [28]. It is also assumed that surface tension is negligible where $\Delta P > \gamma/b$. At time t_{end} the drop bursts resulting in rupture of the gas-liquid interface. The liquid properties of viscosity μ_L, density ρ_L, and subsequently the kinematic viscosity denoted $\nu_L = \mu_L/\rho_L$, along with the surface tension at the gas-liquid interface γ, are used for normalization throughout the manuscript and their values are assumed to remain constant for a given experimental setup.

A. Volume conservation

The gas phase average radius $\bar{a}_1(t)$ is difficult to estimate from experimental data because of the Saffman-Taylor instability [6]. So we instead rely on volume conservation to develop expressions for the transient cross-sectional area of the gas $A_{\text{gas}} = \int_{A_{\text{gas}}} dA$ (with $dA = r\,dr\,d\theta$ a differential area element), which will allow for direct comparison between theory and experiments where in the experiments $A_{\text{gas}} = \sum_i A_{\text{gas}_i}$ and A_{gas_i} is an area element based on an image pixel i. In general, values for the transient gas phase volume V_{gas} depend on the film that is deposited on the top and bottom walls as the liquid is displaced, where the distance measured from the bottom wall to the lower and upper portion of the gas phase are denoted as h_t and h_b, respectively (see Fig. 1 for description), and may not be spatially uniform. But the Bond number is considered small in the problem statement so the variations in the top and bottom films are negligible in this limit and $h_t = h_b$. Dividing the gas volume V_{gas} by the gas area A_{gas} yields an average gas layer thickness $\frac{V_{\text{gas}}}{A_{\text{gas}}} = b - \bar{h}$, where $\bar{h}$ is the (top and bottom) average-radial liquid film thickness spanning the gas region. The liquid volume $V_{\text{liq}} = \pi a_2^2(0)b$ is constant with no simple expression for the area $A_{\text{liq}} = \int_{A_{\text{liq}}} dA$. The total volume $V_{\text{tot}} = V_{\text{gas}} + V_{\text{liq}}$ is equal to $A_{\text{tot}}(t)b$ where we define the change in total volume as being equal to the gas volume $\Delta V_{\text{tot}}(t) = V_{\text{tot}} - V_{\text{liq}} = A_{\text{tot}}b - \pi a_2^2(0)b = V_{\text{gas}}$ where we consider all cross-sectional areas to be uniform in the z direction, and also assume a similar relationship between differential and image pixel based expressions for the total area as there is for the gas area A_{gas}. Note that the gas area and change in total area also share the same initial condition $A_{\text{gas}}(0) = \Delta A_{\text{tot}}(0) = 0$.

The expression relating the change in total volume with the gas volume may be rewritten as $\Delta A_{\text{tot}}b = A_{\text{gas}}(b - \bar{h})$ where ΔA_{tot} and A_{gas} differ by a constant $\frac{b-\bar{h}}{b}$ when considering steady-average films, that is, $\frac{d\bar{h}}{dt} = 0$. A steady film assumption is not physically possible at early times since the total film thickness value is initially equivalent to the plate separation distance. But after a sufficient amount of elapsed time the

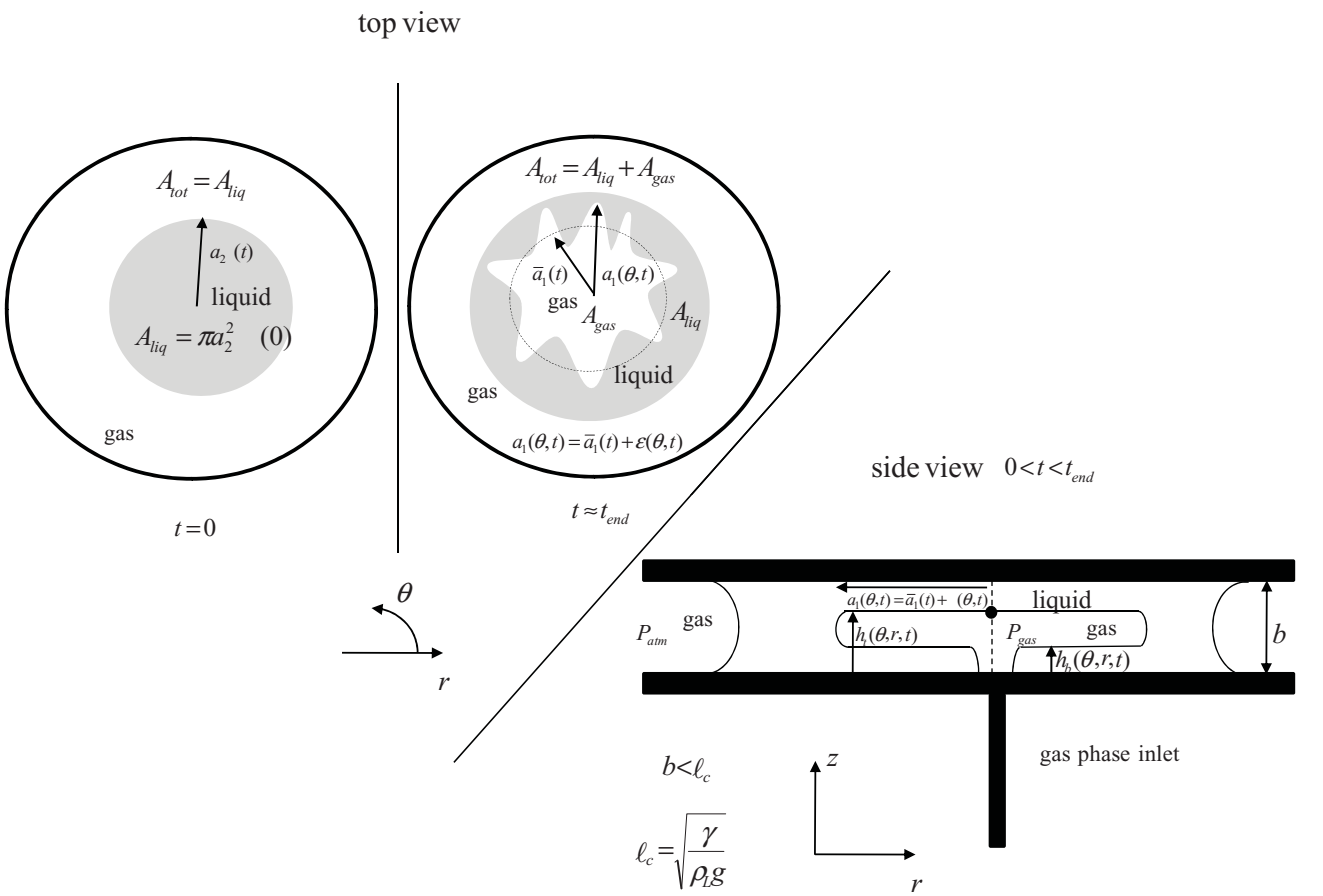

FIG. 1. Top and side view of problem schematic and experimental setup. The top view shows the initial drop configuration at time $t = 0$ and the proposed configuration at later times where a typical fingering instability develops in the azimuthal direction. The radial distance measured from the center to the inner air gas interface a_1 is assumed to be the sum of an average component that is independent of the azimuthal direction and an azimuthally symmetric disturbance radius, i.e., $a_1(\theta,t) = \bar{a}_1(t) + \varepsilon(\theta,t)$. The side view shows the proposed configuration for the top and bottom films.

average film thickness in the region spanning the gas phase is given by

$$\frac{\bar{h}}{b} = 1 - \frac{\Delta A_{\text{tot}}}{A_{\text{gas}}}, \tag{1}$$

where $\bar{h}$ is analogous to $2h_\infty$, the value used in the more traditional liquid film measurement problems. Also, this particular result is analogous to the one derived in [26] for a finite volume of fluid displaced in an initially dry rotating Hele-Shaw cell.

B. Displacement rates

For the gas phase area we assume an empirical relationship for the expansion rate of the form $\dot{A}_{\text{gas}} = \omega A_{\text{gas}}$ (dots denote derivatives with respect to time) and subsequently $\Delta\dot{A}_{\text{tot}} = \omega \Delta A_{\text{tot}}$ due to volume conservation. These expressions are based on experimental observations and [26]. Integration of these equations, with the initial conditions $A_{\text{gas}}(0) = \Delta A_{\text{tot}}(0) = 0$ and $\frac{\dot{A}_{\text{gas}}}{A_{\text{gas}}} = \frac{\Delta\dot{A}_{\text{tot}}}{\Delta A_{\text{tot}}} = \omega$, for $t > 0$, results in expressions for the transient cross-sectional areas,

$$A_{\text{gas}}(t) = C_{\text{gas}}(e^{\omega t} - 1) \text{ and} \tag{2a}$$

$$\Delta A_{\text{tot}}(t) = C_{\text{tot}}(e^{\omega t} - 1). \tag{2b}$$

To determine an expression for ω we analyze the dimensionless momentum conservation equation $\text{Re}^*(\mathbf{u}^*_{t^*} + \mathbf{u}^* \cdot \nabla^* \mathbf{u}^*) = \nabla^* \cdot \boldsymbol{\sigma}^*$ using $1/\omega$, b, and ωb for the time, length, and velocity scales, respectively, and $\mu_L \omega$ for the stress scale $\boldsymbol{\sigma}$ with $\boldsymbol{\sigma} = -P\mathbf{I} + \boldsymbol{\tau}$ where $\boldsymbol{\tau} = \mu_L[\nabla \mathbf{v} + \nabla \mathbf{v}^T]$ is the viscous stress tensor and $\mathbf{I}$ is the identity tensor. In the limit $\text{Re}^* = \frac{\omega b^2}{\nu_L} \ll 1$ we propose that $\omega \propto \Delta P/\mu_L$ based on dimensional analysis and taking into consideration that the fluid is driven by a gas at constant pressure.

Developing empirical relationships for the coefficients C_{gas} and C_{tot} and ω are not straightforward since each depends on the variables μ_L and ΔP and possibly b. Therefore, the main focus on the gas area and the total area rate equations is to determine if the relationship for the characteristic rate $\omega \propto \Delta P/\mu_L$ is accurate within our range of experimental parameters. A more general empirical relationship for ω will be used for comparison with experiments and is a power law of the form

$$\omega = C_\omega \left(N_\omega \frac{\Delta P}{\mu_L} \right)^m, \tag{3}$$

where m is to be experimentally determined. Values of m in the vicinity of unity would reinforce the validity of the main assumptions in this radial flow model.

For the total film thickness an empirical relationship is derived by considering the generic capillary number $\mathrm{Ca}^* = v_{\mathrm{char}}\mu_L/\gamma$. Using this definition with characteristic velocity $v_{\mathrm{char}} = \omega b$ would yield a dimensionless group that is independent of viscosity for $m = 1$. A more precise velocity for the inner annular region is derived by considering the first two nonzero terms in the Taylor expansion of the average gas displacement written in terms of the transient area [Eq. (2a)] yielding the expression $\bar{a}_1(t)\sqrt{\pi} = \sqrt{A_{\mathrm{gas}}} \approx \sqrt{\omega t + O(\omega t)^2}$. Ignoring higher order terms $O(\omega t)^2$ in the expansion suggests that the coefficient for the average velocity and average acceleration are both proportional to $\sqrt{\omega}$ at early elapsed time. Inserting this expression into the capillary number suggests a numerator that scales like $\mathrm{Ca}^* \propto \mu_L\sqrt{\omega} = \sqrt{\mu_L \Delta P}$. We use this result to propose an empirical relationship for the film thickness in terms of the viscosity and pressure of the form

$$\frac{\bar{h}}{b} = C_{\bar{h}}\,(N_{\bar{h}}\mu_L \Delta P)^n\,, \tag{4}$$

where the normalization constant is proportional to the surface tension, that is, $N_{\bar{h}} \propto \gamma$. The power n is to be determined experimentally where measured values of $2n$ in the range $0 < 2n < 2/3$ would suggest the reasoning used to develop the empirical correlation is valid based on previous studies measuring film thickness as a function of the capillary number. A two term power law, in μ and ΔP, would be a much better choice but determining the separate powers from experimental data would be difficult given that we can essentially only measure the cross-sectional areas A_{gas} and A_{tot}.

The functional dependence with ΔP and μ_L that has been proposed for ω and $\bar{h}/b$ are each normalized by $N_\omega = \sqrt{\frac{\rho_L b^3}{\gamma}}$ and $N_{\bar{h}} = \sqrt{\frac{b}{\rho_L \gamma^3}}$, respectively, determined by using dimensional analysis. Experiments are performed to determine the constants and the exponential powers for these expressions.

III. EXPERIMENTS: MATERIALS AND PROCEDURE

A Hele-Shaw cell was created using two circular acrylic plates with a diameter of 100 mm (4 in.) and uniform thickness of approximately 3.2 mm (1/8 in.) set 50, 75, or 100 μm apart on an acrylic stand. Plastic shims (AccuTrex) were placed between the plates to provide the desired gap spacing. In order to insert air into the cell a standard 8-32NC thread was tapped in the center of one plate and a plastic pipe fitting (Cole Parmer) with an inner diameter of 2.4 mm (3/32 in.) was inserted. Air pressure was controlled using a pressure transducer (Marsh Bellofram) and a function generator (Agilent) to provide a step function. Current I from the function generator in the range of $4.8 < I < 10.4$ mA was supplied to the transducer to yield pressure outputs of $\Delta P = 3.5, 7.0$ or 10.5 kPa (0.5, 1.0, or 1.5 psig). There was no observable flexing of the plates used to form the Hele-Shaw cell when tested at these low pressures (less than 15% of 1 atm). An air compressor was used to fill a storage tank to provide pressurized air for the experiments when necessary, and was connected to the transducer with tubing that had an inner diameter of 6.4 mm (1/4 in.). Glycerol-water mixtures were used as the experimental liquid. Kinematic viscosities of roughly 4, 37, and 280 cSt were made using mixtures of 50%, 80%, and 95% glycerol-water (by weight), respectively [29,30]. Based on these viscosities and our other parameters we determine the Reynolds number to be in the range of $10^{-5} < \mathrm{Re}^* < 10^{-1}$. Surface tension for pure glycerol on acrylic is approximately 60 mN/m, yielding values of $\gamma/b \approx$ 1.2 kPa for the smallest gap spacing. Therefore $\Delta P > \gamma/b$ for our range of pressures although the ratio $\gamma/(b\Delta P)$ is approximately one-third for the smallest pressure of 3.5 kPa. Bond numbers are in the range $0.01 < \mathrm{Bo}^* < 0.1$, based on capillary lengths in the range of 1–2 mm where the value varies due to the density difference between the fluid mixtures. The range of normalized correlation parameters are $1 < N_\omega \frac{\Delta P}{\mu_L} < 500$ and $0.1 < N_{\bar{h}}\mu_L \Delta P < 100$ for ω and $\bar{h}/b$, respectively.

Drops with volumes of either 13, 30, or 50 μl were placed at the center of the Hele-Shaw cell by using an Eppendorf syringe. The supply valve from the storage tank to the transducer was opened prior to the signal generator supplying the transducer with a current. As the signal generator began to supply the transducer with a current the transducer allowed the pressurized air to enter the cell through the tapped hole. A CCD camera (PixeLINK) looking normal to the cell from above was used to capture video of the experiment at a minimum of 30 fps at the maximum resolution of 1280 × 1024 pixels and at a maximum of 100 fps at a reduced resolution of 640 × 480. The video captured an experiment from just before the initial injection of the air until a few seconds after the drop burst. Run times for the experiments ranged from less than 0.1 to over 102 s depending on viscosity, providing a minimum of approximately 10 experimental images for analyzing each experiment. The combination of volumes, viscosities, pressures, and gap spacings yielded 51 experiments. Several experiments at small gap spacings, $b <$ 75 μm, with the lowest viscosity fluid of 4 cSt were difficult to perform as the drops were susceptible to meandering or to an instability that occurs along the interface as they are squeezed between the plates [31]. After each experiment the Hele-Shaw cell was disassembled. Water with a small amount of soap was applied to each side of both acrylic plates followed by a thorough rinse with water. A soft towel was used to dry the plates to avoid scratching and the Hele-Shaw cell was reassembled for a new experiment.

A MATLAB program was used to precisely analyze the images. For each image frame the gas area and the total area were measured by calculating and summing local pixel intensities $A_{\mathrm{gas}_i} = \sum_i A_{\mathrm{gas}_i}$ and $A_{\mathrm{tot}_i} = \sum_i A_{\mathrm{tot}_i}$, respectively. There were some initial pixels that were always present due to the pixel intensity of the gas phase inlet and therefore produced a nonzero initial area for the gas phase. Only the frames from the initial injection of air until the first burst were analyzed with the bursting time recorded as t_{end} for these experiments. The area data was used to produce an average film thickness estimate using Eq. (1). A steady-state film value for the average film thickness measurements is defined as the final two to three values for the film thickness being within 10% of one another. No error bars are plotted in the following graphs because none of the data is averaged.

IV. EXPERIMENTS: RESULTS AND DISCUSSION

A. Qualitative results

Figure 2 shows images of drops prior to bursting for a range of pressures and viscosities. The set of top and bottom images represents results of experiments with two different initial volumes of 13 and 50 μl, respectively, with the pressures listed in the left-hand column. In general the Saffman-Taylor instability is always present [6,21]. The amplitude of the fingers appear less pronounced at the lower pressures, for a given volume and viscosity, and tend to become more pronounced through branching and tip splitting events at higher pressures according to the images. Also, the fingering pattern appear to be symmetric for most of the experimental images shown.

The first and second columns of the 13 μl volume experiments show fingering patterns that are qualitatively similar at each pressure. The total cross-sectional area at bursting though does not appear similar with a much larger area in the 4 cSt viscosity and 3.5 kPa experiment versus the 37 cSt and 3.5 kPa one. The remainder of the experiments in the first and second column do appear to have similar total expanded volumes at bursting. A comparison of the first and second column for the 50 μl experiments reveals similar patterns to those seen in the 13 μl experiments, that is, similar fingering patterns at each pressure. Comparing experiments with different volumes and for fixed viscosity, there is qualitatively similar fingering behavior at equivalent pressure values. Also, Comparing the two drop volumes for fixed pressure with varying viscosity shows similar trends of a decrease in the total and gas cross-sectional areas at the bursting event.

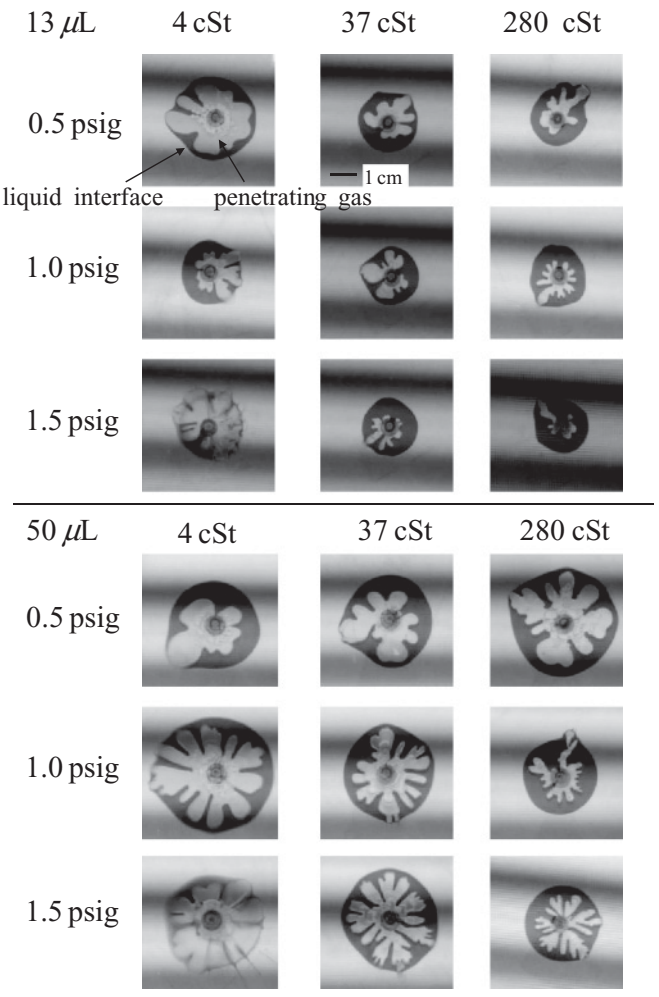

FIG. 2. Images of bursting event for drops in a Hele-Shaw cell. The volume for the upper portion of the figure and lower portion, separated by the line, are 13 and 50 μl, respectively. The viscosity is listed at the top and the pressure in the left-hand column.

B. Quantitative results

Figures 3(a) and 3(b) show semilog plots of the measured gas and the total cross-sectional areas made dimensionless using the constants C_{gas} and C_{tot}, respectively, as functions of elapsed time. The values for the constants are generated from a fit to the equation $A_{\text{gas}} = C_{\text{gas}}(e^{\omega t} - 1)$ and $\Delta A_{\text{tot}} = C_{\text{tot}}(e^{\omega t} - 1)$ using the experimental data. The dotted lines are the plots of the function $e^{\omega t}$ for each of the corresponding experiments. The viscosity is 280 cSt in all of the data shown in these two plots with the other operating parameters described in the legend. At early elapsed times there are errors in the image analysis that are displayed by several values of the dimensionless areas being less than unity for a few sets of experimental results shown in Fig. 3(a). Comparing the two sets of data [Figs. 3(a) and 3(b)] it appears that the dimensionless gas area has a slightly larger range ($1 \leqslant A_{\text{gas}}/C_{\text{gas}} + 1 \leqslant 10^3$) than the change in the total area ($1 \leqslant \Delta A_{\text{tot}}/C_{\text{tot}} + 1 \leqslant 20$). The largest elapsed times occur for a combination of larger fluid volumes and smaller gap spacing.

Figure 3(c) shows the data for the normalized average-total film thickness $\bar{h}/b$ versus elapsed time Δt. The film thickness values, each denoted by a symbol described in the legend, correspond to experiments shown in the previous graph where the viscosity is constant in each at 280 cSt. Most of the data for the average film thicknesses reach a steady value prior to bursting. Some of the points exhibit oscillatory behavior partially due to viscous fingering. But some experiments do appear to show liquid displacements where the ratio of the transient area measurements are indeed oscillatory. All of the data points corresponding to experiments with inlet pressures of 7.0 kPa reach an equilibrium in a much shorter time than the 3.5 kPa inlet pressure experiments, while the data points corresponding to the low-pressure experiments (3.5 kPa) all seem to reach an equilibrium value after approximately 1 s.

Figure 4 displays a summary of the total area and gas area measurements in the form of two plots. Figures 4(a) and 4(b) are log-log plots of normalized $\Delta P/\mu_L$ versus $\text{Re}^* = \omega b^2/\nu_L$ where the Reynolds numbers are determined by using ω derived from the gas and total area data, respectively. Each data set consists of approximately three decades of data with a best fit line also drawn. There is little scatter in the data with a monotonic trend for increasing normalized $\Delta P/\mu_L$ versus $\text{Re}^* = \omega b^2/\mu_L$.

Figure 5(a) shows a log-log plot of normalized $\Delta P/\mu_L$ versus the bursting time, normalized by a combination of the

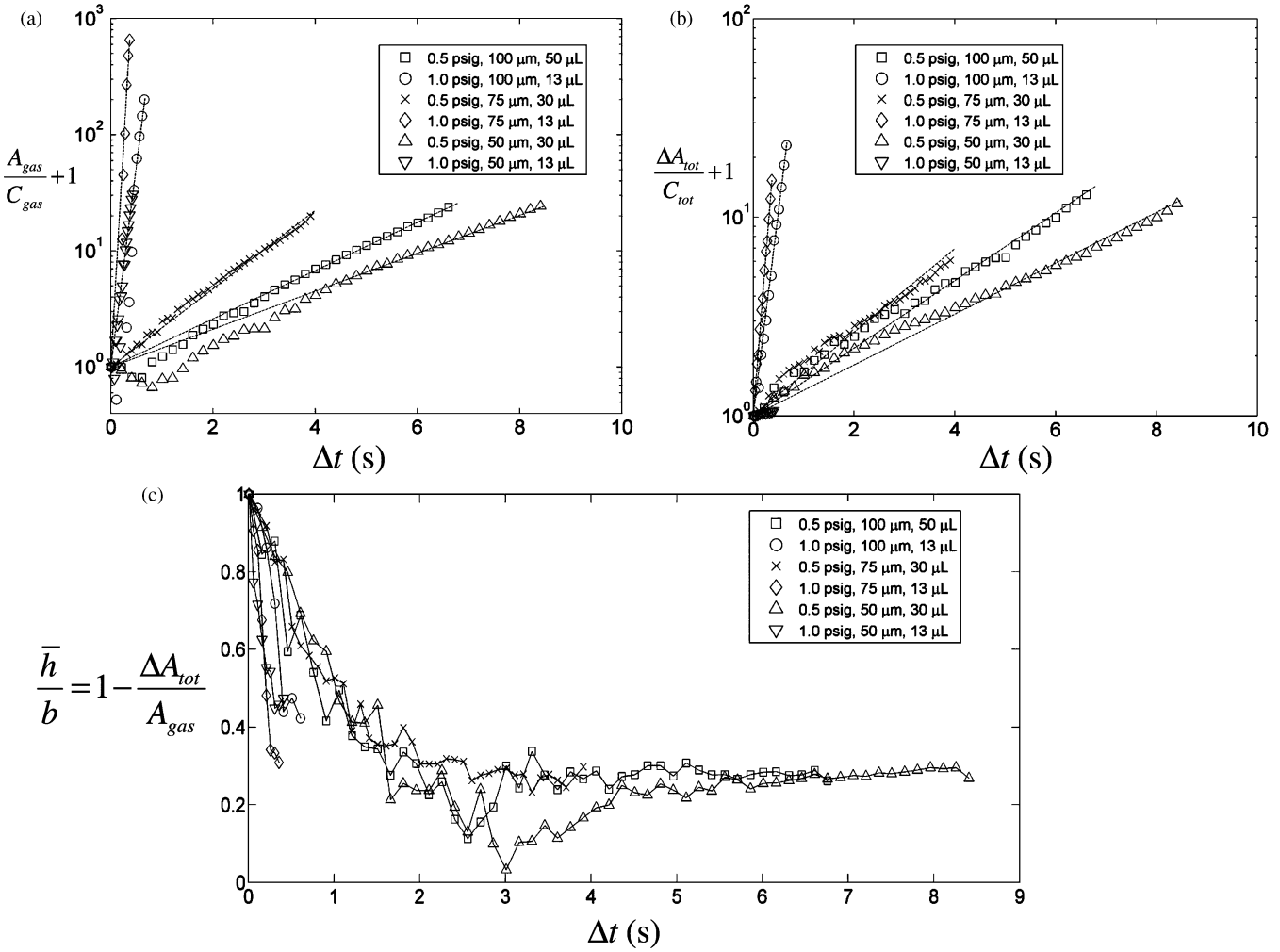

FIG. 3. Semilog plot of (a) $\frac{A_{\rm gas}}{C_{\rm gas}}+1$ and (b) $\frac{\Delta A_{\rm tot}}{C_{\rm tot}}+1$ vs elapsed time for inlet pressures, fluid volumes, and gap spacings as listed in the legend. The viscosity is 280 cSt in each experiment. Lines are drawn through the data representing the best fit curves $e^{\omega t}$. (c) Plot of normalized total average film thickness $\bar{h}/b$ vs elapsed time for inlet pressures, fluid volumes, and gap spacings as listed in the legend. The viscosity is 280 cSt in each experiment. Several experiment do not reach an equilibrium while others display small amplitude oscillatory behavior.

kinematic viscosity, gap spacing, and liquid volume. The data range is fairly robust with the bursting time plotted for over three decades of values. The general trend is a monotonic decrease in the bursting time as either the pressure or gap spacing is increased or by a decrease in the liquid viscosity. The best fit line appears to fit the general trend with several data points from different experiments lying directly on the line.

Figure 5(b) shows the log-log plot of normalized $\mu_L \Delta P$ versus film height calculated using Eq. (1), normalized by the plate separation distance. The range of normalized $\mu_L \Delta P$ spans three decades but the average film thickness only spans one, that is, the minimum average film thickness is approximately one-tenth of the gap spacing suggesting that the films span the range of 5–95 μm. The dotted line is the best fit for all of the data with several data points from different experiments lying on the line. The dispersion in the data is fairly uniform at small and large values of the normalized $\mu_L \Delta P$ parameter with an equal number of points above and below the best fit line.

C. Discussion

In Figs. 3(a) and 3(b) the lines representing the best fits $e^{\omega t}$ appear to fit the data very well for the elapsed time range shown. At early times there is clearly some deviation possibly due to errors in the algorithm used to measure the areas but taken as a whole it appears that the plots are linear suggesting that the radial expansion empirical correlations Eqs. (2a) and (2b) are accurate for the range of parameters tested. The results seem to correspond to the prewet cell experiments of Carrillo *et al.* [26] since these clearly show exponential behavior. The discrepancy between our results and theirs may be due to the fact that the authors plot their data versus a nondimensionalized function $f(t)$, which is used to capture the transient behavior of the rotating motor, instead of the actual elapsed time as we have done. Another possible reason for the discrepancy is the notion that a prewet and dry cell possess different dynamics. Since the less viscous phase fluid displaces the more viscous one then there is some dynamic wetting of the dry-wet region where the liquid and the plates meet. This would suggest that surface tension may in fact be relevant in the results presented

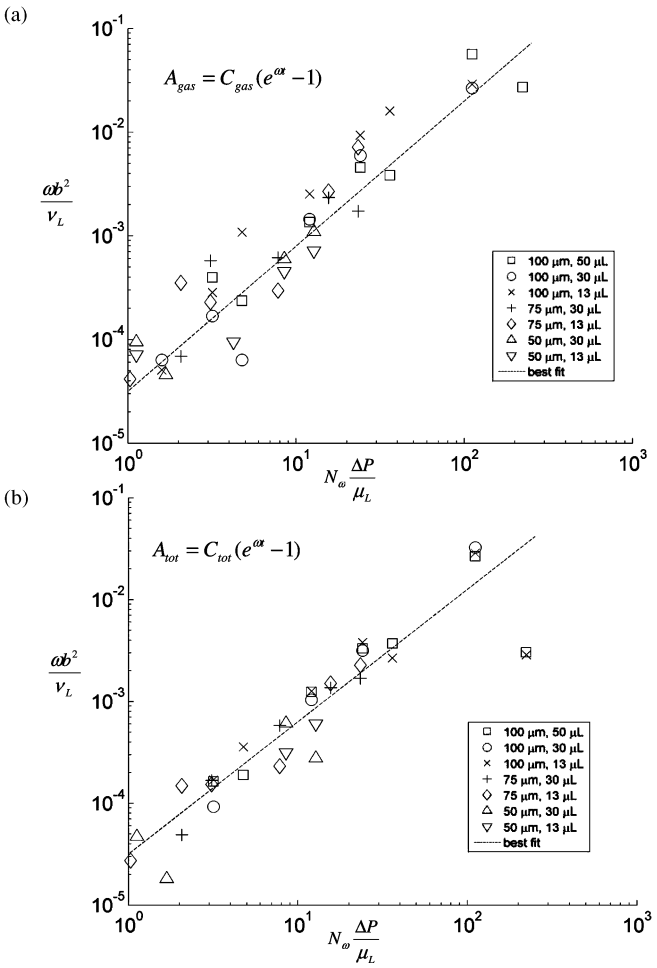

FIG. 4. Log-log plots of Reynolds number $\mathrm{Re}^* = \omega b^2/\nu_L$ vs normalized $\Delta P/\mu_L$ where the characteristic rate ω is measured using either the transient (a) gas or (b) total cross-sectional area fit to the expression $C_i(e^{\omega t} - 1)$ where the i represents either the gas or total area. A best fit line is drawn in each graph.

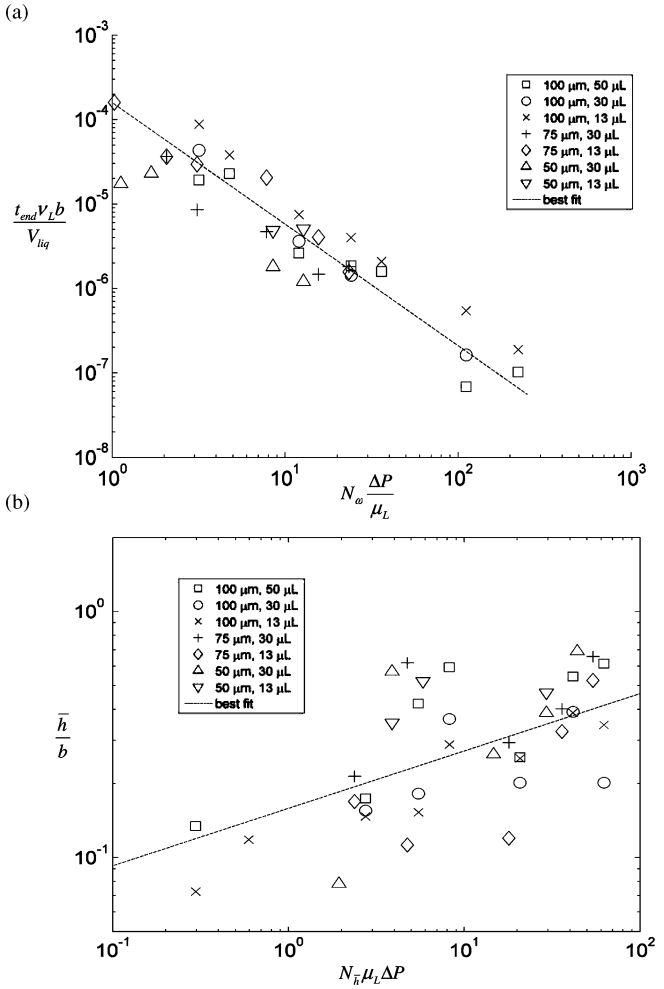

FIG. 5. (a) Log-log plot of $t_{\mathrm{end}}\nu_L b/V_{\mathrm{liq}}$ vs normalized $\Delta P/\mu_L$. (b) Log-log plot of $\bar{h}/b$ vs normalized $\mu_L \Delta P$. A best fit line is drawn in each graph.

here. But since the surface tension does not vary much from one experiment to another then its precise relevance cannot be accurately determined. But the reader should note that Carrillo *et al.* studied a different problem, that is, the *stable* displacement of a liquid annulus, for which a nearly exact analytical formulation can be drawn. The study presented here reduces to the Carrillo *et al.* result when the Saffman-Taylor instability is ignored and average quantities are considered. Although the average fronts are circular and hence the average fluid domain is indeed annular, it is not at all certain that the dynamics of these average magnitudes in actual viscous fingering flows should coincide with the dynamics of the liquid annulus studied in [26].

We continue the discussion with results related to the characteristic rate ω. The values for the exponent m used in the expression for ω [Eq. (4)] based on the gas and total area data are 1.19 and 1.28 and for C_ω are 1.7×10^{-5} and 3.1×10^{-5}, respectively, for the data shown in Figs. 4(a) and 4(b). Therefore our assumption of constant and equivalent characteristic rate ω for the measurements of $A_{\mathrm{gas}}(t)$ and $A_{\mathrm{tot}}(t)$ appears to be accurate. Also the values for each ω appears to be within 20%–30% of unity. The fact that the values are larger than unity suggest that an additional pressure may need to be included in future studies such as capillary pressure γ/b. Also, a more detailed explanation of the behavior near the penetrating gas-displaced liquid region that includes the curvature of the interface in the plane of the plates may provide more accurate results (Ref. [24] provides a review of relevant studies). This would require more detailed analysis of the fingering wavelength since the curvature is directly related to its value, but this is outside the scope of the present study. The range for the constants, normalized by the gap spacing, are $10\,000 < C_{\mathrm{gas}}/b^2 < 40\,000$ and $2000 < C_{\mathrm{tot}}/b^2 < 10\,000$. The constants do not change by one order of magnitude and therefore we believe it would be difficult to determine an accurate correlation between them and the variables ΔP and μ_L.

The data for the burst time [shown in Fig. 5(a)] follows the best fit line fairly well. The bursting time t_{end} is the only empirical expression that appears to involve fluid volume. According to the best fit line, the bursting time t_{end} is proportional to $(\frac{\Delta P}{\mu_L})^{-1.38}$. The absolute value of the exponent is similar to the one determined for the characteristic rate ω suggesting that the product of ωt_{end} is weakly dependent on

$\Delta P/\mu_L$ according to the experiments and therefore mostly depends on the volume and b, that is, $\omega t_{\text{end}} \sim \frac{V_{\text{liq}}}{b^3}$. Given that $\omega \propto \frac{\Delta P}{\mu_L}$ then the time to burst is approximately $t_{\text{end}} \sim O(\frac{\mu_L V_{\text{liq}}}{b^3 \Delta P})$ where we have assumed a power of unity for the empirical relationship between ω and $\frac{\Delta P}{\mu_L}$. This relationship though may fail to capture precise bursting times because the velocity of the leading-penetrating interface may dominate, particularly in the deeply nonlinear regime of the Saffman-Taylor instability.

The final set of data to discuss are the average film thickness results. The main result is that the film does appear to reach a steady-state thickness for our range of parameters according to the data presented in Fig. 3(c). In Fig. 5(b) the plots for the normalized average film thickness follow the monotonic trend shown by the best fit curve. Given the slope and intercept, the best fit curve yields the expression

$$\frac{\bar{h}}{b} = 0.15 \left(\frac{\mu_L \Delta P}{\rho_L^{1/2} \gamma^{3/2}} b^{1/2} \right)^{0.27} \tag{5}$$

for the average film thickness as a function of $\mu_L \Delta P$. Note that the gap spacing appears on both sides of the equation for convenience. Twice the exponent $2n = 0.54$ is lower than what has been predicted for and observed in other systems using similar measurement technique [26] but is relatively close in value to other general studies. The film measurement data, as a whole, also does not show asymptotic behavior as the $\bar{h}/b$ reaches a maximum value of unity. But individually the data does appear to show asymptotic behavior, in particular the 100 μm gap spacing with 13 and 50 μl drop experiments. Overall, it requires about three orders of magnitude change in the normalized $\mu_L \Delta P$ to yield one order of magnitude change in average film thickness for $0.1 < N_{\bar{h}} \mu_L \Delta P < 100$ according to Fig. 5(b). The measurement of thin films of gas (thick liquid films) are a surprising result of the experiments. The results for t_{end} when combined with Eqs. (2a) and (5) are useful for determining the volume of gas $V_{\text{gas}} = A_{\text{gas}}(b - \bar{h})$ that penetrates the liquid droplet as it expands in a radial Hele-Shaw cell prior to bursting.

V. CONCLUSION

In this paper the displacement of a more viscous phase fluid by a less viscous phase is studied in a radial Hele-Shaw geometry. The less viscous phase fluid is air and the more viscous phase is a mixture of glycerol-water at various concentrations. The air is injected into the liquid phase at constant pressure for three different volumes of liquid and the experiment continues until the gas breaks through the interface. The average film thickness, gas phase and total areas, and bursting time are measured by analyzing images of the experiments.

The experimental results suggest the gas phase and liquid phase areas expand exponentially with respect to time, analogous to [26] for the problem of a fluid displaced in a rotating Hele-Shaw cell. The measured film thicknesses span 5% –95% of the the gap spacing over the range of pressures and viscosities. The bursting times appear to follow a monotonic trend and scale with the fluid volume.

In the future it will be beneficial to perform additional experiments varying the surface tension either by using surfactants or other fluids. It also may be useful to perform experiments under nonisothermal conditions to understand more details of the finger formation and fluid displacement in nonideal systems.

ACKNOWLEDGMENTS

The authors would like to thank G. M. "Bud" Homsy and T. P. Witelski for their insightful comments and suggestions. Useful comments were also provided by a referee that should be acknowledged. The authors would also like to acknowledge the NC Space Grant for supporting this research and for providing undergraduate support for A. R. White.

[1] M. Blunt, F. J. Fayers, and F. M. Orr, Energy Convers. Manag. **34**, 1197 (1993).
[2] V. S. Ajaev and G. M. Homsy, J. Colloid Interface Sci. **240**, 259 (2001).
[3] D. H. Cho, Chem. Eng. Sci. **26**, 1235 (1971).
[4] V. K. Dhir, AIChE J. **47**, 813 (2001).
[5] D. Banerjee and V. K. Dhir, ASME J. Heat Transfer **123**, 271 (2001).
[6] P. G. Saffman and G. I. Taylor, Proc. R. London Ser. A **245**, 312 (1958).
[7] M. B. Gratton and T. P. Witelski, Phys. Rev. E **77**, 016301 (2008).
[8] D. A. Reinelt and P. G. Saffman, SIAM J. Sci. Stat. Comput. **6**, 542 (1985).
[9] L. Schwartz, Phys. Fluids **29**, 3086 (1986).
[10] J.-M. Vanden Broeck, Phys. Fluids **26**, 2033 (1983).
[11] D. Bensimon, L. P. Kadanoff, S. Liang, B. I. Shraiman, and C. Tang, Rev. Mod. Phys. **58**, 977 (1986).
[12] R. G. Cox, J. Fluid Mech. **14**, 81 (1962).
[13] K. V. McCloud and J. V. Maher, Phys. Rep. **260**, 139 (1995).
[14] F. P. Bretherton, J. Fluid Mech. **10**, 166 (1961).
[15] F. Fairbrother and A. E. Stubbs, J. Chem. Soc. **1**, 527 (1935).
[16] G. I. Taylor, J. Fluid Mech. **10**, 161 (1961).
[17] J.-D. Chen, J. Colloid Interface Sci. **109**, 341 (1986).
[18] C.-W. Park and G. M. Homsy, J. Fluid Mech. **139**, 291 (1984).
[19] D. A. Reinelt, J. Fluid Mech. **183**, 219 (1987).
[20] E. Meiburg, Phys. Fluids A **1**, 938 (1989).
[21] L. Paterson, J. Fluid Mech. **113**, 513 (1981).
[22] H. Kim, T. Funada, D. D. Joseph, and G. M. Homsy, Phys. Fluids **21**, 074106 (2009).

[23] G. M. Homsy, Annu. Rev. Fluid Mech. **19**, 271 (1987).
[24] T. Maxworthy, Phys. Rev. A **39**, 5863 (1989).
[25] C.-W. Park, S. Gorell, and G. M. Homsy, J. Fluid Mech. **141**, 257 (1984).
[26] L. Carrillo, J. Soriano, and J. Ortín, Phys. Fluids **11**, 778 (1999).
[27] E. Álvarez-Lacalle, J. Ortín, and J. Casademunt, Phys. Rev. E **74**, 025302(R) (2006).
[28] J. M. Smith and H. C. Van Ness, *Introduction to Chemical Engineering Thermodynamics*, 4th ed. (McGraw-Hill, New York, 1987).
[29] R. C. Ernst, C. H. Watkins, and H. H. Ruwe, J. Phys. Chem. **40**, 627 (1936).
[30] P. N. Shankar and M. Kumar, Proc. R. Soc. London Ser. A **444**, 573 (1994).
[31] T. Ward, Phys. Fluids **18**, 093101 (2006).